

Absorption and elastic and inelastic reflection of spin-polarized low-energy electrons from Fe(110)

M. S. Hammond,* G. Fahsold, and J. Kirschner

*Freie Universität Berlin, Institut für Experimentalphysik, Arnimallee 14, D-1000 Berlin 33,
Federal Republic of Germany*

(Received 18 September 1991)

The spin dependence of low-energy electron absorption and reflection from ferromagnetic Fe(110) is investigated using the normalized difference between the absorption (or reflection) of electrons polarized parallel and antiparallel to sample magnetization. The resulting absorption and reflection spin asymmetries are found to be reciprocal to each other, with their magnitudes related in a simple manner. Structure in the spin asymmetries is identified with features in the spin-split bulk band structure and is thus found to be related to the spin-polarization fine structure of secondary electrons emitted from the same surface. The general structure of the spin asymmetry as a function of incident energy is dominated by elastic-scattering events, although inelastic scattering is found to play a major role in determining the sign and magnitude of the absorbed and total (energy-integrated) reflected asymmetries. Furthermore, the existence of nonzero elastic-reflection asymmetries indicates the existence of spin-split unoccupied energy bands up to 50 eV above the vacuum level. Inelastic-scattering spin asymmetries show a 2-eV energy-loss feature that is identified as due to the creation of Stoner excitations in the ferromagnet. This feature is determined to be surprisingly insensitive to the incident electron energy (from 0 to 50 eV) and angle (from 0° to 65° from the normal) in contrast to predictions of a recent theory of spin-polarized electron scattering in ferromagnets.

I. INTRODUCTION

Of the many surface analytical microscopies,¹ three particularly promising examples are low-energy electron microscopy (LEEM),² scanning low-energy electron diffraction (LEED) microscopy,³ and scanning electron microscopy with polarization analysis (SEMPA).⁴ In LEEM, which uses the sample as the cathode in an immersion objective lens, the sample is illuminated by a parallel beam of low-energy electrons, and the backscattered electrons are imaged. Scanning LEED microscopy uses the diffracted beams from a low-energy scanning electron microprobe to image structures and defects of surfaces. In SEMPA, a high-energy (2–30 keV) scanning electron microprobe is used to excite secondary electrons from the sample. The low-energy secondary electrons thus created are spin analyzed as a function of microprobe position to image the micromagnetic domain structure of the sample. In LEEM, scanning LEED microscopy, and SEMPA, surface sensitivity is achieved by virtue of the small escape depth for low-energy electrons, which in turn depends on the details of elastic and inelastic electron-scattering processes inside solids and the transmission of low-energy electrons from the solid into the vacuum.⁵ In addition, the effect of these scattering processes on the spin of either the incoming or outgoing electrons is important for SEMPA and especially for future spin-polarized versions of LEEM.⁶ A more thorough and quantitative knowledge of low-energy scattering processes, including the spin and energy dependencies, for “hot” electrons up to several tens of eV above the vacuum level is thus desirable in order to extract the maximum amount of information from these

surface microscopies.

In this paper, we seek quantitative insights into the low-energy scattering processes of spin-polarized electrons in ferromagnetic materials by measuring the normalized difference in the (absorbed or reflected) current for incident electrons polarized either parallel or antiparallel to sample magnetization. We present here comprehensive measurements of this normalized difference (which we will henceforth refer to as the “spin asymmetry”) for absorption and reflection of low-energy electrons incident on Fe(110) over a range of incident energies (0–50 eV) and angles (0°–65°). All reflected spin-asymmetry measurements are angle integrated and we have measured the spin asymmetry in the total (energy-integrated) reflected yield, the elastically reflected current, and the (energy-differentiated) inelastically reflected current. Unpolarized electron reflection⁷ and absorption^{8–11} measurements have proven useful for determining the effect of band structure on electron-scattering processes, as well as identifying major features in the unoccupied electronic band structure of solids and their surfaces. Spin-polarized work by Siegmann, Pierce, and Celotta¹² using a ferromagnetic metallic glass sample, measured the spin asymmetry in the absorbed and reflected current. These measurements were concerned mainly with the asymmetry near the zero crossing in the absorbed current rather than the low-energy asymmetries. Tamura *et al.*¹¹ have calculated the elastic reflected current spin dependence for Fe(001), demonstrating the usefulness of spin-polarized electron reflection and absorption measurements for studying the unoccupied band structure of ferromagnetic single crystals. Thus we have chosen a single-crystal [Fe(110)] sam-

ple, with which we are able to demonstrate the importance of the spin-split bulk band structure and its coupling to the vacuum (so-called "LEED states") in determining the spin dependence of elastic and inelastic electron scattering.

Reference 11 also makes a case for measuring the more "easily accessible" absorbed, or target, current; however, we have chosen to measure both the absorbed and reflected currents for several reasons. First, we wish to demonstrate explicitly the reciprocal nature of the absorbed and reflected spin asymmetries. This reciprocity is explained in terms of a simple detailed balancing argument. Second, by measuring the reflected current, we can separate out, and directly measure, the contribution of the elastic channel to the total current spin asymmetry. This allows us to forego any assumptions concerning the effect of inelastic scattering on the total reflected (or absorbed) spin asymmetries. And finally, we can also measure the inelastic spin asymmetry as a function of energy loss only by including the reflected current. It so happens that the structures that are measured directly in the inelastic spin asymmetry lend further insight into the relationship between the elastic reflected and absorbed spin asymmetries.

Spin-polarized electron-energy-loss spectroscopy (SPEELS) has been used to measure the angle-resolved spin dependence of low-energy electron scattering from Ni(110) (Refs. 13–15) and Fe(110).¹⁶ These experiments have been performed using spin-polarized incident electrons (generally at one fixed energy), and measured either both the energy *and* spin of the scattered electrons (the so-called "complete" experiment)^{15,16} or the energy-resolved intensity asymmetry for incident electrons of opposite spin direction.^{13,14} The results of these experiments established the importance of electron-hole creation and spin-flip (exchange) scattering in ferromagnetic materials, and confirmed the existence of Stoner excitations.¹⁷ However, these experiments, being angle resolved, provide little indication of the magnitude of the Stoner excitation creation phenomenon as a function of incident electron energy and angle for arbitrary electron **k** vector. By measuring the *angle-integrated* inelastic reflected current, we are able to reach conclusions concerning the general importance of Stoner excitations for spectroscopies and microscopies with poor or no angular resolution, as well as the dependence of these excitations on incident electron energy and angle. As a result, we have a data base for comparison to the most modern theories of spin-polarized electron-energy-loss scattering, and this comparison finds the current theories in need of improvement or modification.

While a close inspection of the absorption and reflection of low-energy electrons is obviously of interest for LEEM and LEED microscopy (as well as a host of other nonmicroscopic surface spectroscopies), SEMPA utilizes spin-polarized low-energy secondary electrons emitted by high-energy electron excitation. The data presented here concern, as well, the understanding of the polarization of secondary electrons emitted from ferromagnets. Typically, the polarization of secondary electrons emitted from a ferromagnetic sample is considered,

in a first approximation, to result from two contributions. The first is a result of the true secondary-electron cascade and reflects the bulk sample magnetization, with a polarization enhancement below about 20 eV.¹⁸ The second contribution to the secondary-electron polarization is a crystal-face-dependent polarization fine structure.^{19–21} The reported measurements concerning low-energy electrons *incident* upon a ferromagnetic sample have important implications for techniques using secondary electrons *emitted* from ferromagnetic samples as well. The secondary-electron spin-polarization enhancement described above has been qualitatively explained as being due to inelastic-scattering events suffered by low-energy electrons as they make their way to the surface,²² and is thus related to the inelastic-scattering experiments described here. More importantly, it has been demonstrated theoretically that the fine structure in secondary-electron emission spectra²³ and polarization spectra²⁴ is determined by the bulk band structure and its coupling to LEED states, and is therefore related to the low-energy spin-dependent absorbed and reflected current. The correspondence of the secondary-electron polarization fine structure to the absorbed- (and reflected-) current spin asymmetry has also recently been demonstrated experimentally.²⁵ This correspondence will be detailed further in the following discussion of experimental results. Up to now, all calculations of the secondary-electron polarization spectrum have dealt with either the cascade or the fine-structure contribution; however, only a qualitative separation of the two contributions to the total polarization is presently possible. The correspondence of the measured absorbed current spin asymmetry to the secondary-electron polarization fine structure should make possible a more quantitative separation of the polarization fine structure from the cascade polarization. This is especially important since the shape of the cascade polarization enhancement is able to provide direct information about the electron-electron interaction in metals.¹⁵

II. EXPERIMENTAL ASPECTS

The apparatus used to measure absorbed- and reflected-current asymmetries is shown schematically in Fig. 1. A 0–50-eV spin-polarized primary electron beam is obtained from a negative-electron-affinity GaAs_{1-x}P_x photocathode irradiated with circularly polarized light from a Kr⁺-ion laser. Polarization magnitudes of 25–30% are typical and can be directly verified by a LEED-type polarimeter.²⁶ After a 90° deflection and focusing, the electron beam emerges, transversely polarized, through the center of a three-grid hemispherical LEED analyzer. Energy resolution of the incident electron beam is limited to several tenths of an eV due to compromises made between energy spread and intensity losses. The first hemispherical grid (closest to the sample) is connected to the final electron gun lens element and can be biased to provide a field-free region between it and the sample. The second and third grids can then serve as the collector for the total backscattered current or, by biasing the second grid and collecting from the third, can

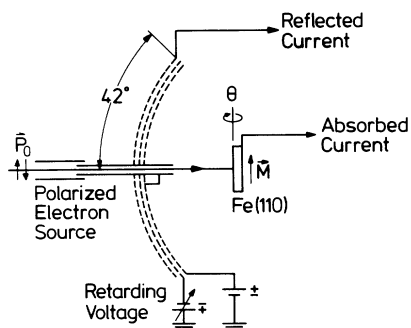


FIG. 1. Schematic of apparatus for measuring the absorbed and angle-integrated reflected current and current spin asymmetries.

be operated in the energy high-pass mode to study the reflected current as a function of scattered electron energy loss. With such a high-pass energy filter (retarding-field energy analyzer) it is possible to measure directly the elastic fraction of the reflected current. In addition, for a given, fixed incident electron-beam energy, one can obtain an angle-integrated electron-energy-loss spectrum by ramping the voltage on the second grid and numerically differentiating the current collected on the third grid as a function of pass energy. The hemispherical grids have an acceptance angle of 84° , and so by “total backscattered current” we are referring to the energy-integrated reflected current collected in the resulting solid angle. The deleterious effects of this limited collection angle will be discussed in more detail below. The absorbed current is simply obtained by measuring the current flow from the sample to the ground.

The sample is a single crystal of iron, cut to expose the (110) face. The sample is cleaned with cycles of Ar^+ -ion sputtering, heating to 700°C and occasional heating in oxygen.²⁷ Surface cleanliness was monitored with Auger-electron spectroscopy. The crystal is mounted on a soft iron magnet yoke and oriented such that the sample can be remanently magnetized along the $\langle 100 \rangle$ easy axis of magnetization. The sample-magnet-yoke assembly is mounted such that the incident electron spin-polarization vector and the sample magnetization vector are parallel (or antiparallel) to one another and are both perpendicular to the incident-electron-beam direction. The sample can be rotated on the [100] direction to vary the incident angle of the polarized electron beam. A Pockels cell is used to change the polarization of the Kr^+ -ion laser light between positive and negative helicity, thus reversing the polarization of the incident electron beam. This modulation is carried out at approximately 1 kHz, making possible the use of a lock-in technique to detect the resulting difference in the (absorbed and reflected) current when the spin polarization of the incident beam is reversed. Data are also collected with the sample magnetization reversed to allow for the subtraction of instrumental or nonmagnetic (e.g., spin-orbit-induced) asymmetries. Care is taken to assure that stray

magnetic fields or other spurious effects do not contribute to the measured asymmetry.

The spin-dependent absorption and reflection results reported here are expressed in terms of a normalized asymmetry $A(E_0)$ for a primary-electron-beam energy E_0 of 0–50 eV:

$$A(E_0) = \frac{1}{P_0} \frac{I^\uparrow - I^\downarrow}{I^\uparrow + I^\downarrow}, \quad (1)$$

with $P_0 = 0.25$ the incident-beam polarization magnitude and $I^\uparrow = I^\uparrow(E_0)$ [$I^\downarrow = I^\downarrow(E_0)$] the absorbed or reflected current for incident beam of energy E_0 and polarization parallel (antiparallel) to the sample majority-spin direction. The absorbed currents I_a^\uparrow and I_a^\downarrow form the absorbed-current asymmetry $A_a(E_0)$ and, likewise, the total reflected currents I_r^\uparrow and I_r^\downarrow form the total reflected-current asymmetry $A_r(E_0)$. Figures 2(a) and 3(a) show the spin-averaged absorbed and total reflected currents, respectively, as functions of primary-electron energy E_0 for a series of incident angles ranging from $\theta = 0^\circ - 65^\circ$ from sample normal, taken in steps of $\sin\theta = 0.033$. For the same conditions, Fig. 2(b) shows the absorbed-current spin asymmetry $A_a(E_0)$ as a function of primary-electron energy, and Fig. 3(b) shows the total reflected-current spin asymmetry $A_r(E_0)$. The currents shown in Figs. 2(a) and 3(a) have been normalized to the current measured at the highest energy (for ease of viewing), and have not been normalized to the actual beam current as a function of beam energy. Note that, as shown by the sign of the vertical scale in Fig. 3(b), the reflected current asymmetries are inverted to facilitate comparison with the absorbed current asymmetries. It can immediately be seen that the absorbed- and reflected-current asymmetries are roughly reciprocal; that is, they are opposite in sign, and maxima in the absorbed current asymmetries correspond to minima in the reflected current asymmetries. When comparing Figs. 2(b) and 3(b), it is obvious that the two sets of data differ somewhat, although they should be expected to possess similar shapes, aside from sign and magnitude (see discussion). This is due to the limited acceptance angle of the collection grids, as briefly mentioned above. The effects of lost reflected intensity is most obvious at lower energies and the larger angles of incidence in the reflected current asymmetry measurements presented in Fig. 3(b). At normal incidence, the specularly scattered electrons are not collected due to the placement of the electron-gun optics in the center of the collection grids, resulting in a loss of asymmetry in the low-energy range ($E_0 = 1 - 6$ eV). At angles larger than approximately 20° , the specular beam is no longer collected by the grids, and the main lobe of electrons scattered by dipolar fields is again mostly lost. This lost reflected intensity results in the departure of the reflected asymmetry curves from reciprocity with the absorbed asymmetry curves above $\sin\theta \approx 0.33$. Considering the experimental difficulties confronted in attempting to collect all of the reflected electrons, the ab-

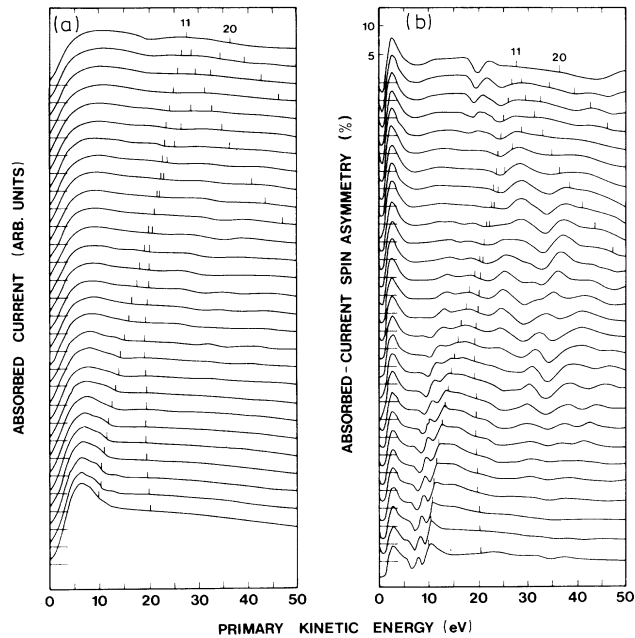


FIG. 2. Absorbed current (a) and absorbed current spin asymmetry A_a (b) from Fe(110) for incident angles of $\theta=0^\circ$ (top) to $\theta=65^\circ$ (bottom) in steps of $\sin\theta=0.033$. The calculated energetic positions of LEED beam emergences are labeled with tic marks just above the curve to which they correspond.

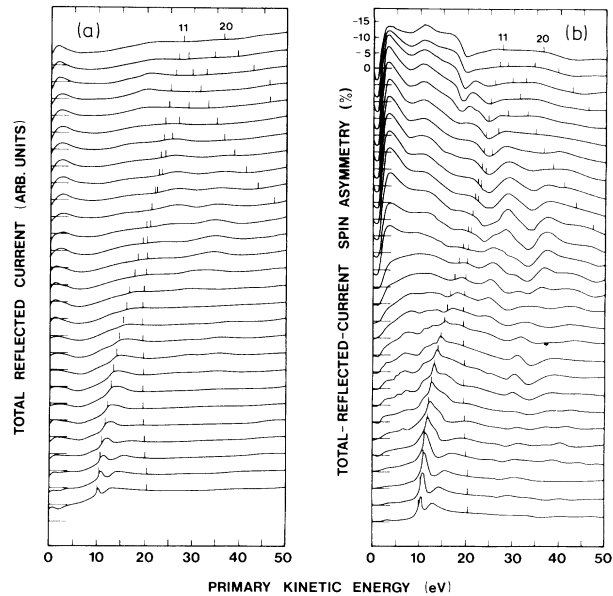


FIG. 3. As Fig. 2, but for the total reflected current (a) and total reflected current spin asymmetry A_r (b). Note that the vertical scale for the spin asymmetry has been inverted for ease of viewing.

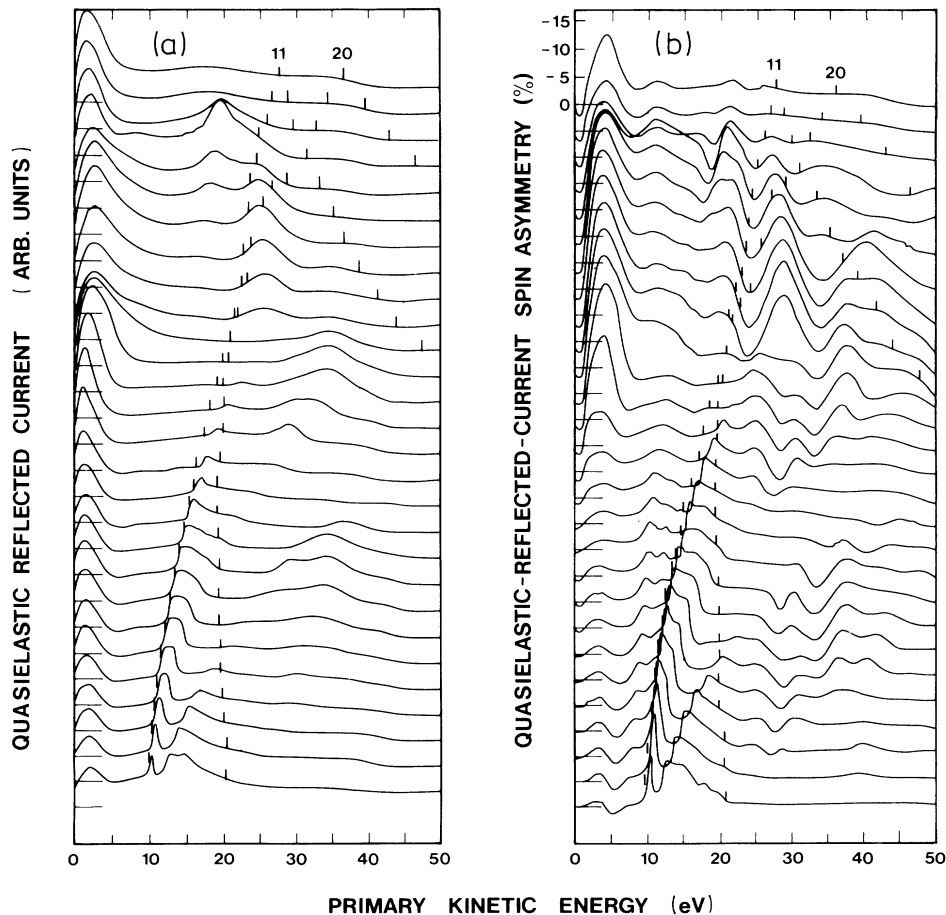


FIG. 4. As Figs. 2 and 3, but for the quasielastic (as defined in the text) reflected current (a) and quasielastic reflected current spin asymmetry A_{re} (b). Note that, as in Fig. 3, the vertical scale for the spin asymmetry has been inverted.

sorbed current may appear to be the preferred quantity to measure; however, measuring the reflected current provides us with the possibility to distinguish between the elastic and inelastic contributions to the spin asymmetry. For these reasons, we have chosen to measure both the absorbed current and the angle-integrated reflected current (elastic and inelastic) asymmetries.

Figures 4(a) and 4(b) show the quasielastic reflected current and current asymmetry [with inverted scale, as in Fig. 3(b)], respectively, for the same electron incident angles and energies as in Figs. 2 and 3. These data were taken with the hemispherical grid assembly operated in the energy high-pass mode. The second hemispherical grid was biased (see Fig. 1) such that only electrons suffering less than 1.5-eV energy loss were accepted (we therefore refer to these electrons as “quasielastic”), while all other experimental conditions were the same as those used to collect the data in Fig. 3. Looking at the quasielastic reflected asymmetry $A_{re}(E_0)$ curves in Fig. 4(b), one sees features similar to those in the total reflected asymmetry $A_r(E_0)$ of Fig. 3(b). In particular, for the lower incident angles in the upper half of Fig. 4(b), there is a prominent peak around 4 eV with asymmetry values between 15% and 20% and a series of peak and valley structures between 20 and 30 eV that correspond to similar, but less dramatic, structures in Fig. 3(b). Also at higher angles in the lower half of both Figs. 3(b) and 4(b) there are a series of features between 10 and 20 eV that appear to exhibit some angular dispersion. It can be deduced from these observations that much of the structure in $A_r(E_0)$ is contributed by the elastic portion of the

reflected current (see Sec. III).

To study the spin dependence of the inelastically scattered electrons, the hemispherical grid analyzer can also be used as a retarding field electron energy analyzer. Numerical differentiation of the current collected while ramping the high-pass voltage on the second grid (for a constant incident electron energy E_0) results in an electron energy distribution curve and a reflected spin asymmetry $S(E)$ (as a function of scattered electron energy E), as shown in Figs. 5(a) and 5(b), respectively. The data shown in Fig. 5 were taken for $\theta=15^\circ$ and an incident electron energy of $E_0=45$ eV. Similar data were collected for incident electron energies of $E_0=7-50$ eV. The energy distribution curves appear very typical, possessing an elastic peak some 1 eV wide (due mostly to the energy resolution of the retarding field analyzer arrangement) and a broad low-energy secondary-electron peak. The inherent limitations imposed by energy resolution and error propagation during numerical differentiation render extremely fine structure in the energy distribution curve practically unobtainable; however, the inelastic spin asymmetry $S(E)$ provides a rather large, broad single feature at small (≈ 2 eV) energy loss and some very broad, less intense features at greater energy loss that are clearly resolved. The interesting point here, and this will be discussed in detail below, is that $S(E)$ is *not* featureless.

III. DISCUSSION OF RESULTS

The most basic observation that can be made from the absorbed- and reflected-current asymmetry curves shown in Figs. 2(b) and 3(b) is that the two sets of curves display similar structure (aside from the exceptions due to limited collection angle, as noted above), but differ in sign and magnitude. That is, the absorbed and reflected asymmetries are reciprocal to one another. This is simply a consequence of charge conservation and detailed balancing. The total reflected current I_r^\uparrow (I_r^\downarrow) resulting from an incident electron beam of energy E_0 and spin polarization parallel (antiparallel) to the sample magnetization direction can be expressed in terms of the polarized incident current (assuming, for the time being, that $P_0=1$) \mathcal{J}^\uparrow (\mathcal{J}^\downarrow), and a reflection coefficient ρ^\uparrow (ρ^\downarrow) (where $\rho^{\uparrow(\downarrow)}$ includes all of the reflected current, i.e., the backscattered and secondary electrons):

$$I_r^\uparrow = \rho^\uparrow \mathcal{J}^\uparrow \quad (I_r^\downarrow = \rho^\downarrow \mathcal{J}^\downarrow), \quad (2)$$

where $\rho^{\uparrow(\downarrow)}$ is also a function of E_0 . Likewise, an absorption coefficient $\alpha^{\uparrow(\downarrow)}$ can be defined. By virtue of charge conservation, $\alpha^\uparrow + \rho^\uparrow = 1$ ($\alpha^\downarrow + \rho^\downarrow = 1$). The measured asymmetries can therefore be expressed in terms of these theoretical reflection and absorption coefficients (once again taking into account $P_0 < 1$) as

$$A_r(E_0) = \frac{1}{P_0} \frac{\rho^\uparrow - \rho^\downarrow}{\rho^\uparrow + \rho^\downarrow} \quad (3)$$

and

$$A_a(E_0) = \frac{1}{P_0} \frac{\alpha^\uparrow - \alpha^\downarrow}{\alpha^\uparrow + \alpha^\downarrow}. \quad (4)$$

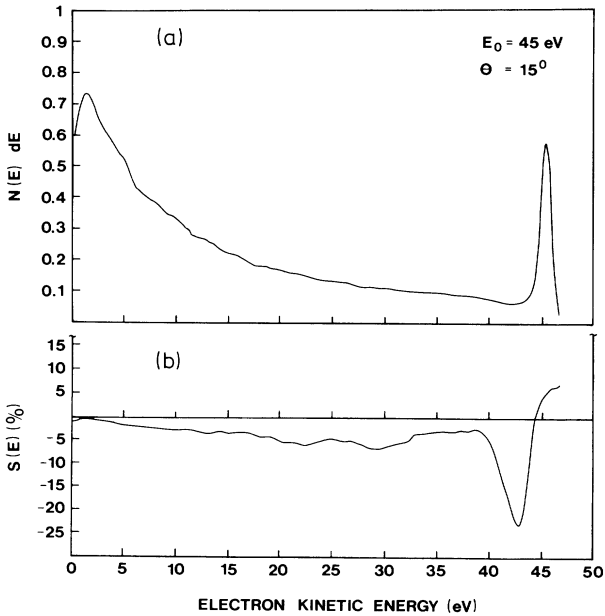


FIG. 5. The reflected electron energy distribution (a) and the energy-dependent reflected electron spin asymmetry $S(E)$ (b) for an incident electron beam energy of 45 eV and incident angle of 15° from normal. Note the large negative feature at approximately 2-eV energy loss and the nonzero asymmetry for most of the energy-loss range.

Combining Eqs. (3) and (4) with the charge-conservation requirement gives

$$\frac{A_a}{A_r} = -\frac{\rho}{\alpha}, \quad (5)$$

where $\rho = (\rho^\uparrow + \rho^\downarrow)/2$ and $\alpha = (\alpha^\uparrow + \alpha^\downarrow)/2$ are the average (or spin-independent) reflection and absorption coefficients. According to Eq. (5), the absorbed- and reflected-current asymmetries should possess the same features while having opposite sign, and therefore contain the same information. Equation (5) also shows that the magnitudes of the two asymmetries are simply related by the ratio of the absorption and reflection coefficients.

Tic marks in Figs. 2 and 3 locate the calculated energetic positions of LEED beam emergence thresholds. Only at $\theta = 0^\circ$ does an entire family of LEED beams (the $\{11\}$ family, for example) emerge at the same energy. It has been noted in earlier work that the emergence of LEED beams has only small influences on the absorbed and reflected currents.¹¹ Insensitivity to emergent LEED beams is found here in the absorbed- and reflected-current asymmetries also, excepting the emergence of the (20) beams at large angles ($\theta > 40^\circ$). It is difficult to know, *a priori*, whether these features at high angles of incidence are really due to the emergence of the (20) beams or if there is some band-structure feature in this region that is responsible. Theoretically, LEED beam emergences do have an effect on the current asymmetries;²⁸ however, these are very sharp features occurring over very narrow energy ranges and could be easily obscured by the experimental energy resolution of the present apparatus.

Now we will discuss in more detail how the absorbed and reflected currents and asymmetries depend on the crystal's bulk band structure and its coupling to the vacuum. To facilitate the following discussion, asymmetry and current curves for several incident angles from Figs. 2 and 3 have been reproduced more clearly in Figs. 6 and 7. Figures 6(a) and 6(b) show the absorbed-current spin asymmetry $A_a(E_0)$ and the (spin-averaged) absorbed current, respectively, for incident angles of $\theta = 0^\circ$, 15° , and 30° . Figures 7(a) and 7(b) show similarly the total reflected-current spin asymmetry $A_r(E_0)$ and the reflected current, respectively. The reciprocity between the absorbed- and reflected-current asymmetries is most clearly seen for the case of $\theta = 15^\circ$. For reasons detailed in the experimental description, lost (uncollected) reflected current results in a smaller asymmetry for $\theta = 0^\circ$ and 30° and a lack of reciprocity, especially below a primary-beam energy of about 10 eV. In Figs. 6(b) and 7(b), the absorbed and reflected currents have been normalized to the incident beam current as a function of primary-beam energy. In the case of the reflected currents, the limited collection angle makes an absolute calibration of the vertical scale impossible, and the normalization of the reflected currents by a small incident current yield unreliable data below ≈ 1 eV.

The absorbed and reflected currents behave in the general fashion expected for metals. The reflected fraction of the current starts out large and drops to a broad

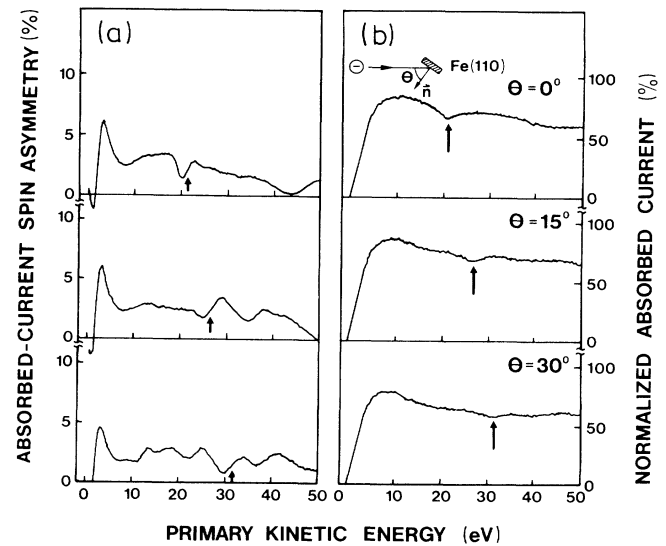


FIG. 6. Absorbed current spin asymmetry (a) and normalized absorbed current (b) for the selected incident angles 0° , 15° , and 30° . Vertical arrows mark the energetic positions of local minima in the absorbed current and the corresponding energy in the spin asymmetry of the same angle.

minimum around 5-eV incident energy. This is in agreement with the work of MacRae and Caldwell,²⁹ who show that the reflection of electrons below 5 eV is dominated by elastic reflection from the surface potential barrier. As the incident energy is further increased above 5 eV, the reflected fraction of the incident beam grows again due to the increase in inelastic-scattering events.

Besides these general features, the spin-averaged ab-

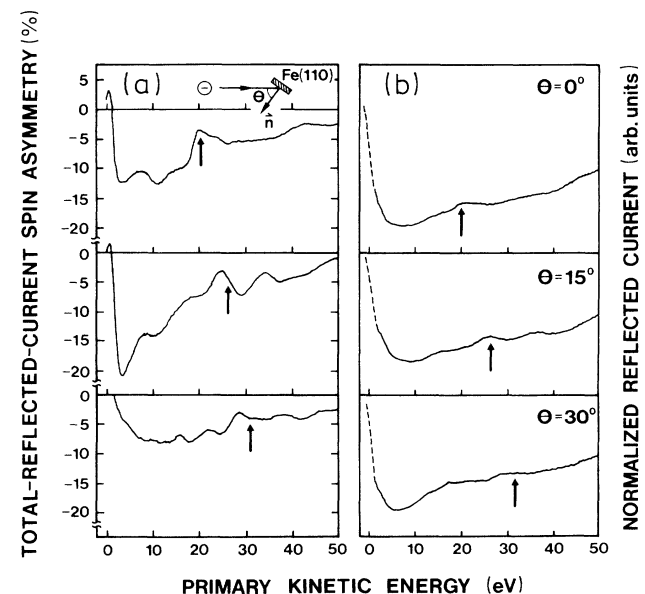


FIG. 7. As Fig. 6, but for the total reflected current spin asymmetry (a) and the normalized total reflected current (b). Here the vertical arrows mark the energetic positions of relative maxima in the reflected current.

sorbed and reflected currents [Figs. 6(b) and 7(b), respectively] also contain information about the bulk band structure of the Fe(110) crystal. At normal incidence there is a peak in the reflected current at approximately 20-eV incident energy (marked by an arrow) that corresponds to a local minimum in the absorbed current (also marked by an arrow). This is clear evidence of a gap in the band structure, and it occurs close to the position of the band gap along the [110] direction calculated for a nearly-free-electron dispersion relation with an inner potential of 12 eV. A band gap results in a decrease in the absorbed current, and a concomitant increase in the reflected current, due to the lack of empty bulk states to which incident electrons can couple. For a general combination of kinetic energy and angle of incidence there will exist a multiplicity of bands into which incident, and out of which emitted electrons, can couple. That is, absorption and emission in a general direction of reciprocal space involves states located throughout the reduced Brillouin zone, and wave matching at the surface will "weight" the various final-state components differently. In addition, energy losses suffered by off-normal incident electrons outside the crystal via long-range electric fields associated with elementary excitations within the solid ("dipole scattering"), combined with refraction upon entering the crystal, will result in incident electrons coupling into different directions in k space depending on the energy loss suffered. Thus one cannot simply assume, for off-normal (as well as for normal) incidence, that features are only due to band gaps, and a full LEED theoretical calculation of the elastic reflection coefficient is necessary for the definitive identification of features. Such LEED calculations have previously been performed for the Fe(100) surface by Tamura *et al.*¹¹ Theoretical work is currently being undertaken for the Fe(110) surface for off-normal angles corresponding to those presented here.²⁸

A band gap will result in a strong feature in reflected- and absorbed-current spin asymmetries due to the spin splitting of the bulk band structure. Because minority-spin electron states are shifted upward in energy with respect to majority-spin states, there will exist an excess of empty minority states at the low-energy end of a band gap and an excess of majority states at the high-energy end. This situation results in the sharp features seen in both asymmetries at approximately 20 eV for $\theta=0^\circ$. The arrows in Figs. 6(a) and 7(a) mark the energetic position of the minimum (maximum) in the spin-averaged absorbed (reflected) current. Note that the inflection points in the asymmetries occur at a lower energy than in the currents. This is because the negative (positive) excursion in the absorbed (reflected) current asymmetry occurs at the low-energy end of the band gap, where there exist more empty minority states than majority states for electron transmission into the solid. Other minima (maxima) in the absorbed (reflected) current have been marked for $\theta=15^\circ$ and 30° , and the corresponding energetic positions are marked in the absorbed- and reflected-current asymmetries in Figs. 6(a) and 7(a). As mentioned above, at these angles of incidence, features can no longer be assigned simply to band gaps due to the complicated nature

of the off-normal diffraction process. However, the features marked in the absorbed and reflected currents correspond to much more intense (and more easily identifiable) features in the absorbed and reflected asymmetries, making a comparison between experiment and theory much less ambiguous. A further important result of these asymmetry measurements is the observation that the asymmetries are nonzero over the entire energy range studied. This observation leads us to conclude that the bulk band structure of iron is spin split, to some extent, as far as 50 eV above the vacuum level, in agreement with Tamura *et al.*¹¹

As noted in the Introduction, the absorbed- and reflected-current asymmetries have recently been demonstrated to be related to the spin-polarization fine structure of low-energy secondary electrons.²⁵ The spin polarization, as a function of emission energy and angle, of secondary electrons excited by high-energy (2 keV) primary electrons from the same Fe(110) sample in an earlier experiment³⁰ is shown in Fig. 8. The polarization is along the majority-spin direction. The polarization exhibits a low-energy enhancement and an angle-dependent fine structure. This fine structure in the polarization, which has been identified with the spin-split bulk band structure,¹⁸ concerns us here. If the structure in the asymmetries in Figs. 6(a) and 7(a) are in fact a result of the bulk band structure, then there should be a correspondence between these structures and the secondary-electron polarization fine structure.

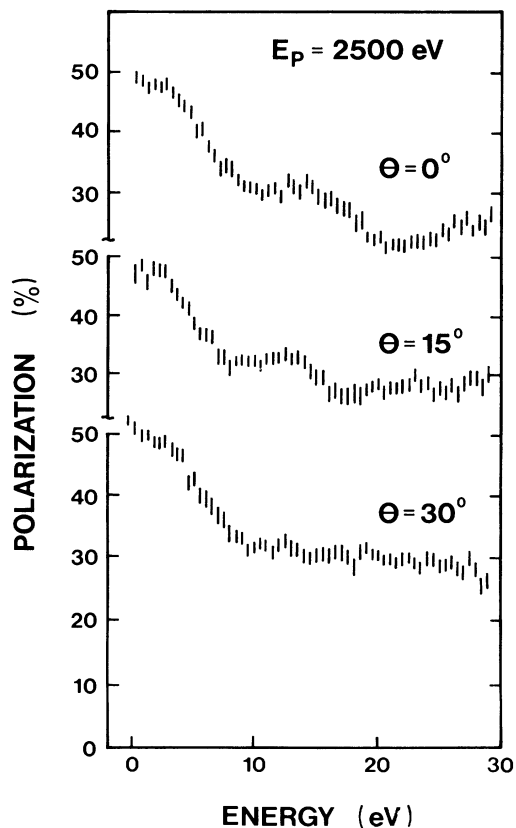


FIG. 8. Spin-polarization distributions for secondary electrons emitted at angles of 0° – 30° from Fe(110).

In general, the absorbed-current asymmetry is observed to be positive and the reflected-current asymmetry negative. That is, *majority*-spin primary electrons result in larger *absorbed* current than *minority*-spin primary electrons. This may, at first sight, appear to be in contradiction to the majority-spin polarization of secondary electrons *ejected* at similar energies; however, it is important to realize that the transmission of incident low-energy electrons into the crystal is essentially the time reversal of the emission of low-energy electrons originating inside the crystal. Consideration of time-reversal symmetry requires that the absorbed-current spin asymmetry (not the reflected-current asymmetry) be related to the secondary-electron polarization fine structure. Under time reversal, the momentum and spin of an electron are reversed, while its mass and charge remain the same; however, the magnetization of the sample is also reversed, keeping the relative direction of electron spin and sample magnetization unchanged (i.e., a majority-type electron remains majority type under time reversal). Therefore, any net spin imbalance present in the transmission of spin-polarized electrons into a ferromagnetic solid ("in-coupling" of electrons from free-electron vacuum states into spin-split bulk Bloch states) at some energy will also be present (with the same sign) in the emission of electrons ("out-coupling" of electrons from spin-split bulk Bloch states into free-electron vacuum states) at that same energy. Thus, comparison of the spin-polarized secondary-electron-emission measurements shown in Fig. 8 with the absorbed-current spin asymmetries of Fig. 6(a) more clearly demonstrates the complementary nature of these two measurements. In keeping with the requirements of time-reversal symmetry, the secondary-electron emission angles are compared to the incident angles in the absorbed current. It can be seen that maxima and minima in the absorbed-current asymmetry correspond to the maxima and minima in the secondary-electron polarization fine structure. A positive feature at 3–4 eV, a valley just below 10 eV that increases in sharpness as the angle (of incidence or emission) increases, and a dip at 20 eV that is present only for normal incidence or emission are the more prominent structures in the two sets of data. The similarities between secondary-electron polarization fine structure and absorbed-current asymmetry further suggests that the latter is also determined by the spin-dependent bulk band structure. The crucial determinant of the structure in both of these quantities is the coupling of the bulk crystal electron states to the vacuum electron states, i.e., LEED states, and therefore both quantities can be calculated by LEED theory.^{11,24}

A direct, quantitative comparison of absorbed-current spin asymmetry and secondary-electron polarization fine structure using the data in Figs. 6(a) and 8 did not prove to be straightforward. This is most likely because of the realistic differences in the sources of the two sets of electrons involved. On the one hand, secondary electrons are emitted from a continuum source of unbound states within the crystal. Thus secondary-electron emission depends on energy losses suffered by electrons on their way to the surface of the crystal at energies above the detected

energy E_0 . Likewise, the polarization of these same electrons is determined by spin-dependent scattering events within the secondary-electron cascade at energies above E_0 . Therefore, the fine structure present in the secondary-electron polarization is weighted differently at different energies due to the nonconstant nature of the cascade polarization. On the other hand, incident low-energy electrons are absorbed at their particular incident energy E_0 , so that the absorbed asymmetry is governed by the spin characteristics of the wave matching at this particular energy. Furthermore, it is possible that some electrons incident at E_0 are absorbed (or reflected) at lower energies due to dipole scattering energy losses suffered outside the crystal. This effect further complicates the situation for off-normal geometries due to refraction effects. So, while secondary-electron emission and low-energy electron absorption are related by time-reversal symmetry, the practical experimental limitations pertaining to the separation of these complicating effects makes a quantitative comparison of these two quantities difficult.

Since LEED states are the determining factor in the structure of the absorbed and reflected asymmetries, one would expect that elastic scattering of electrons is the most important contribution to this structure. That this is true can be readily seen in Fig. 9, which shows the quasielastic reflected-current spin asymmetry $A_{re}(E_0)$ (a) and the normalized quasielastic reflected current (b) in the same manner as the absorbed and total reflected asymmetries and currents are presented in Figs. 6 and 7, respectively. A comparison of the quasielastic reflected spin asymmetry $A_{re}(E_0)$ in Fig. 9 with the total reflected spin asymmetry $A_r(E_0)$ in Fig. 7 quickly leads to several conclusions. (For purposes of comparison, it is easiest to consider $\theta = 15^\circ$, where the effects of finite collection angle are minimized.) First, the major peak and valley structures in $A_r(E_0)$ (e.g., the large negative feature below 10 eV, the dip around 20 eV, and the increase towards positive asymmetry near 50 eV) are reproduced in

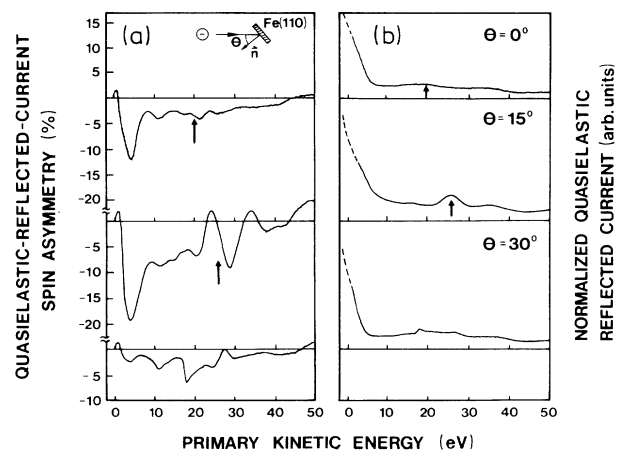


FIG. 9. As Figs. 6 and 7, but for the quasielastic reflected current spin asymmetry (a) and the normalized quasielastic reflected current (b).

$A_{re}(E_0)$, indicating that inelastically reflected electrons contribute little in the way of new structure to $A_r(E_0)$. Secondly, the features in Fig. 9(a) are stronger, (i.e., they exhibit larger peak-to-valley excursions) than those in $A_r(E_0)$, demonstrating that the inelastic contribution to $A_{re}(E_0)$ tends to be smaller on average than the elastic contribution. Thirdly, $A_{re}(E_0)$ is generally shifted to lower absolute values of asymmetry than $A_r(E_0)$. One can conclude from these observations that elastically scattered electrons are responsible, in the main, for the features in absorbed- and total-reflected-current asymmetries. Inelastically scattered electrons tend to diminish the magnitude of the features in $A_r(E_0)$ and $A_a(E_0)$ and add an overall offset to the total asymmetries [negative for the case of $A_r(E_0)$]. From these observations, one cannot conclude that the inelastically scattered electrons contribute no structure at all to the total asymmetry, only that they contribute no new or significant structure, and that they tend to contribute a negative asymmetry to the total reflected spin asymmetry that does not vary dramatically with incident energy between 0 and 50 eV.

In contrast, Tamura *et al.* have stated that much of the information in the elastic reflected current may be extracted from the absorbed current.¹¹ This can be understood by considering the total reflected current I_r as a simple sum of the elastic reflected current I_{re} (which is the sum of the LEED beam intensities, and thus is calculable by LEED theory) and the inelastic reflected current I_{ri} , which accounts for all electrons reflected with energy $E < E_0$ and at arbitrary angles. Assuming an incident electron current of unit intensity, the absorbed current can then be written $I_a = (1 - I_{re} - I_{ri})$. As a result of the angular and energetic integration implicit in I_{ri} , it can be assumed that I_{ri} varies only slowly compared to I_{re} . Therefore, the second derivative (with respect to the incident electron energy) of the absorbed current I_a'' will give roughly the negative of the second derivative of the elastic reflected current $-I_{re}''$. The success of the preceding analysis, of course, depends on the validity of the assumption that I_{ri} does not contribute significantly to the structure of the absorbed current's dependence on incident electron energy. This appears to be a reasonable assumption when considering the absorbed current,¹¹ however, the situation concerning the spin dependence of absorbed and reflected current, as shown in the preceding paragraphs, is not so simple. To make any definitive statement about the exact role of inelastic scattering in the spin asymmetries, one must measure directly the inelastic electrons. Therefore, our ability to perform energy-resolved reflected asymmetry measurements, such as those in Fig. 5(b), is essential to obtaining a complete picture of the elastic and inelastic processes involved in low-energy electron scattering.

Referring back to Fig. 5(b), two noteworthy features in the inelastic asymmetry $S(E)$ are apparent. First, there is a very large negative peak at approximately 2-eV energy loss. Second, at larger energy loss there is still some asymmetry. The large negative peak centered around an energy loss of 2–2.5 eV is certainly the most prominent feature, and is present for all incident beam energies.

This peak shows that minority-type incident electrons create more reflected electrons with energy losses around 2 eV than do majority-type incident electrons. The 2-eV energy loss suffered preferentially by minority electrons can be explained by the creation of Stoner excitations. Stoner excitations are electron-hole pairs of opposite-spin character. The energy of the excitation is given by the energy difference between the hole below the Fermi level and the electron above the Fermi level. These excitations can be created by electron-electron exchange scattering, where an incident electron scatters into an empty state above the Fermi level and ejects an electron of opposite spin from below the Fermi level. The ejected electron will then have the energy of the incident electron minus the energy of the Stoner excitation. In ferromagnetic materials, the spin splitting of the band structure creates a situation where minority electrons are much more likely to create Stoner excitations than majority electrons,¹⁵ and these excitations will be peaked in energy around the exchange splitting energy (≈ 2 eV in Fe). While the spin of the outgoing electron cannot be measured in the present experiment, previous results¹⁶ have demonstrated that spin-flip scattering (i.e., the creation of Stoner excitations) is of major importance in off-specular inelastic scattering in Fe(110).

The asymmetry at energy losses greater than 5 eV is small, but it is not zero and it possesses some very gentle structure. To understand this second point, it is convenient to compare the quasielastic asymmetry $A_{re}(E_0)$, with $S(E)$. Figure 10 shows a composite of $A_{re}(E_0)$ (as a function of incident electron energy) at $\theta = 15^\circ$ and the inelastic asymmetry $S(E)$ (as a function of scattered electron energy) at $\theta = 15^\circ$ for a series of incident energies E_0 . The incident energy for each $S(E)$ curve is marked by a circled vertical bar at the beginning ($E = E_0$) of that curve. The vertical arrows in this figure mark major peaks in the quasielastic asymmetry. As can be seen, these peaks in $A_{re}(E_0)$ correspond to smaller features in the inelastic asymmetries. This slight mirroring of the elastic asymmetry in the asymmetry of inelastically scattered electrons can be explained by inelastic double-scattering events of the type "elastic diffraction followed by energy loss" and "energy loss followed by elastic diffraction." Hence, inelastically scattered electrons *do* contribute to the absorbed- and total-reflected-current spin dependence, however little. Such double-scattering events apparently do not contribute to the inelastic asymmetry for energy losses of greater than about half of the primary energy. This is consistent with low-energy spin-polarized electron-energy-loss results,³¹ which show that, regardless of the initial polarization of the incident electron beam, at sufficient energy losses there is little or no memory of the primary-beam polarization direction.

An interesting and unexpected result of the inelastic asymmetries is the insensitivity of the 2-eV Stoner excitation peak to incident energy. Figure 11 is a plot of the absolute peak size of this 2-eV Stoner peak for incident energies $E_0 = 7-54$ eV and incident angle of $\theta = 5^\circ, 10^\circ, 15^\circ$, and 30° . Peak size is defined here as the asymmetry at an energy loss of 2.5 eV [i.e., $S(E = E_0 - 2.5 \text{ eV})$]

corrected for the background (or offset) created by the asymmetry value of the elastic peak. Even though there is a great deal of scatter in the data, there is no convincing evidence, over the energy range studied, of a strong decrease in size of the Stoner peak as the primary energy is increased, or of any systematic variation with the primary-electron angle of incidence. The solid line in Fig. 11 is merely the result of a least-squares fit of all the data by a straight line, showing only a slight decrease of peak size at higher primary energies. Also, at energies below 10 eV there is a decrease [more easily visible in Fig. 10(b)], perhaps as a result of the large increase of the reflection coefficient leading to a decrease in the ratio between the probabilities for exchange scattering and long-range dipole scattering. The scatter in the data could arise from several different sources, namely error propagation in the numerical differentiation process, errors arising from the offset subtraction procedure (used to determine relative peak heights above background), or real variations in the Stoner excitation probability with incident energy and angle. At any rate, the heights of the peaks attributed here to Stoner excitations are almost always between 15% and 30%. The crucial point is that this insensitivity of the Stoner excitation peak to the

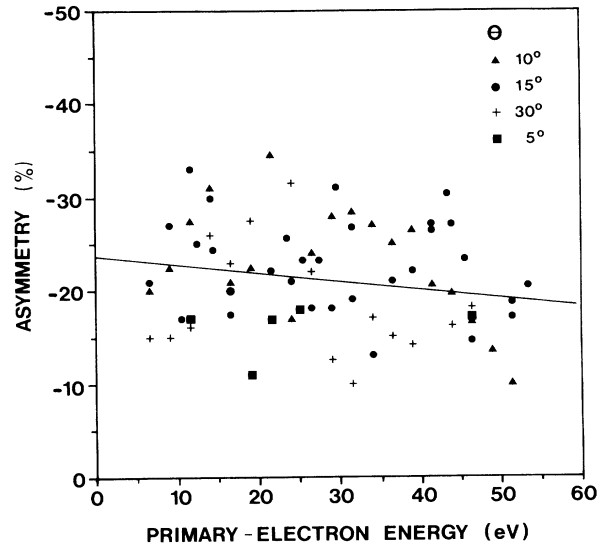


FIG. 11. The magnitude of the Stoner loss feature in $S(E)$ (for an energy loss of 2.5 eV) as a function of incident energy for several different angles of incidence. The solid line represents the results of a least-squares fit of all the data shown.

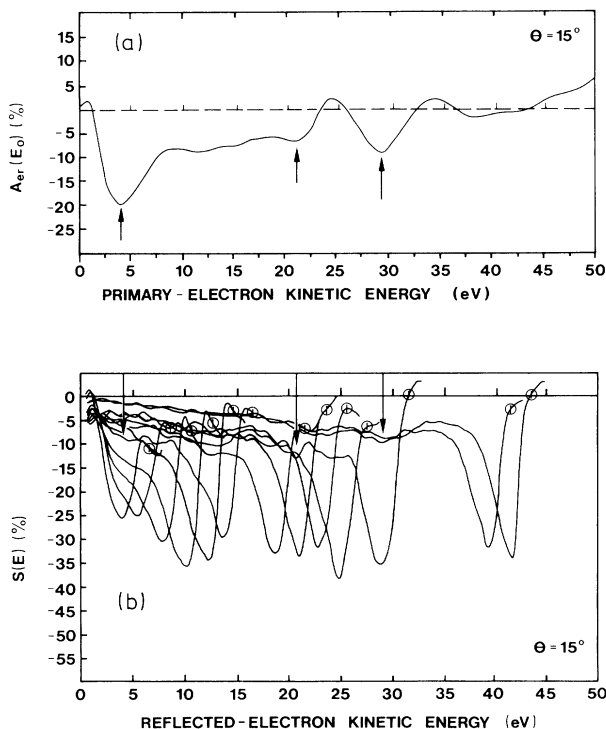


FIG. 10. The quasielastic reflected current spin asymmetry A_{re} (a) as a function of incident energy (see Fig. 9) for an incident angle of 15° , and the energy-dependent reflected electron spin asymmetries $S(E)$ for selected incident energies and the same angle of incidence (the incident energy for each curve is marked by a circled vertical bar). The arrows mark features in A_{re} and the corresponding features in $S(E)$, as discussed in the text.

primary-electron energy runs contrary to predictions arising from recent theories of spin-dependent inelastic electron scattering.^{32,33}

The theoretical works of Bocchetta, Tosatti, and Yin³³ and Glazer and Tosatti³² calculate the "spin-flip" (exchange) and "non-spin-flip" (direct) transition rates for inelastically scattered electrons in ferromagnetic materials. Scattering events that produce spin-flip transitions correspond to the creation of Stoner excitations. The transition rates are proportional to the imaginary part of the forward-scattering amplitudes, which are calculated using the Green's-function formalism with a statically screened Coulomb interaction. The results, described by the authors as purely qualitative, show a sharply decreasing rate for exchange scattering (Stoner excitation creation) for increasing primary-electron energy, and this is clearly at odds with the measurements presented in Fig. 10. The current theory of spin-dependent electron energy losses is built on several extreme simplifications. First, very simple, idealized band structures are used. Omitted band-structure matrix element effects have been cited by Glazer and Tosatti³² as a possible reason for disagreement between theory and experiment at energies of less than 18 eV in the case of Ni. Second, the role of the surface and of spin-orbit coupling are ignored. While the latter simplification may be fairly good for low-atomic-number cases such as Fe and Ni, the current results have shown that the surface (via LEED states) plays an important role in the spin dependence of low-energy electron reflection and absorption. It is impossible at this stage of the theoretical development to determine whether the problem lies within the severity of the above simplifications or an inapplicability of this theoretical approach to the scattering of low-energy electrons in the near-surface region.

IV. CONCLUSIONS

The present spin-asymmetry measurements from a single-crystal ferromagnetic sample have demonstrated the reciprocity of the total-reflected- and absorbed-current spin asymmetries. This reciprocity allows one to monitor the experimentally-more-accessible target current to obtain band-structure information. Features in the absorbed and total reflected asymmetries are found to be due principally to elastic single-scattering events and to depend on the spin-split bulk band structure. The band structure of iron is seen to be spin split up to 50 eV above the vacuum level. The spin polarization of secondary electrons emitted from the same Fe(110) sample exhibits fine structure that corresponds to the structure in the absorbed and reflected asymmetries. The structures in both the polarization fine structure and the asymmetries are identified as spin-split band-structure effects and demonstrate the time-reversal symmetry between the absorption and emission of low-energy electrons.

Reflected-current measurements provide the possibility to study separately the elastic and inelastic contributions to the total asymmetry. In particular, the contribution to the inelastic asymmetry that has been identified as being a result of Stoner excitation creation has shown that Stoner excitations are an observable phenomenon, regardless of the angular resolution. Furthermore, the Stoner contribution is seen to be insensitive to the incident angle or energy of the primary electrons over the ranges studied, pointing out the need for additional theoretical work to describe the scattering of low-energy electrons near the surface.

ACKNOWLEDGMENTS

This work was supported by the Deutsche Forschungsgemeinschaft through Sonderforschungsbereich 6. Helpful discussions with J. Krewer, R. Feder, and K. Koike are gratefully acknowledged.

*Present address: Schmidt Instruments, Inc., 2476 Bolsover, Suite 234, Houston, TX 77005.

¹See, for example, *Physical Aspects of Microscopic Characterization of Materials*, edited by J. Kirschner, K. Murata, and J. A. Venables (Scanning Microscopy International, Chicago, 1987).

²W. Telieps and E. Bauer, *Ultramicroscopy* **17**, 57 (1985).

³T. Ichinokawa, Y. Ishikawa, M. Kemmochi, N. Ikeda, Y. Hosokawa, and J. Kirschner, *Surf. Sci.* **176**, 397 (1986).

⁴K. Koike and K. Hayakawa, *Jpn. J. Appl. Phys.* **23**, L187 (1984).

⁵C. J. Powell, *J. Electron. Spectrosc. Relat. Phenom.* **47**, 197 (1988).

⁶E. Bauer (private communication).

⁷E. N. Sickafus, *Phys. Rev. B* **16**, 1436 (1977); **16**, 1448 (1977).

⁸R. C. Jaklevic and L. C. Davis, *Phys. Rev. B* **26**, 5391 (1982).

⁹S. A. Lindgren, L. Wallden, J. Rundgren, and P. Westrin, *Phys. Rev. B* **29**, 576 (1984).

¹⁰S. A. Komolov and L. T. Chadderton, *Surf. Sci.* **90**, 359 (1979).

¹¹E. Tamura, R. Feder, J. Krewer, R. E. Kirby, E. Kisker, E. L. Garwin, and F. K. King, *Solid State Commun.* **55**, 543 (1985).

¹²H. C. Siegmann, D. T. Pierce, and R. J. Celotta, *Phys. Rev. Lett.* **46**, 452 (1981).

¹³J. Kirschner, D. Rebenstorff, and H. Ibach, *Phys. Rev. Lett.* **53**, 698 (1984).

¹⁴D. L. Abraham and H. Hopster, *Phys. Rev. Lett.* **62**, 1157 (1989).

¹⁵H. Hopster and D. L. Abraham, *Phys. Rev. B* **40**, 7054 (1989).

¹⁶D. Venus and J. Kirschner, *Phys. Rev. B* **37**, 2199 (1988).

¹⁷J. Kirschner, *Phys. Rev. Lett.* **55**, 973 (1985).

¹⁸M. Landolt, in *Polarized Electrons in Surface Physics*, edited by R. Feder (World Scientific, Singapore, 1985).

¹⁹E. Kisker, W. Gudat, and K. Schröder, *Solid State Commun.* **44**, 591 (1982).

²⁰H. Hopster, R. Raue, E. Kisker, G. Güntherodt, and M. Campagna, *Phys. Rev. Lett.* **50**, 70 (1983).

²¹R. Allenspach, M. Taborelli, and M. Landolt, *Phys. Rev. Lett.* **55**, 2599 (1985).

²²D. R. Penn, S. P. Apell, and S. M. Girvin, *Phys. Rev. Lett.* **55**, 518 (1985).

²³R. Feder and J. B. Pendry, *Solid State Commun.* **26**, 519 (1978).

²⁴E. Tamura and R. Feder, *Phys. Rev. Lett.* **57**, 759 (1986).

²⁵M. S. Hammond, G. Fahsold, K. Koike, and J. Kirschner, *Vacuum* **41**, 500 (1990).

²⁶J. Kirschner, in *Polarized Electrons at Surfaces*, edited by H. Lotsch, Springer Tracts in Modern Physics Vol. 106 (Springer-Verlag, Berlin, 1985).

²⁷J. Kirschner, *Surf. Sci.* **138**, 191 (1984).

²⁸J. Krewer, R. Feder, G. Fahsold, M. S. Hammond, and J. Kirschner (unpublished).

²⁹E. G. MacRae and C. W. Caldwell, *Surf. Sci.* **57**, 77 (1976).

³⁰J. Kirschner and K. Koike (unpublished).

³¹J. Kirschner and S. Suga, *Solid State Commun.* **64**, 997 (1987).

³²J. Glaser and F. Tosatti, *Solid State Commun.* **52**, 905 (1984).

³³C. J. Bocchetta, E. Tosatti, and S. Yin, *Z. Phys. B* **67**, 89 (1987).